Quantifying Wettability Effects on Multiphase Flow in Carbonate and Sandstone Reservoirs

Moustafa Dernaika[1*] and *Shehadeh Masalmeh*[2]

[1] SLB, Reservoir Performance Evaluation, Abu Dhabi, UAE
[2]ADNOC HQ, Upstream, EOR Department, Abu Dhabi, UAE

Abstract. Prediction of oil recovery from reservoir rocks requires a robust understanding of multiphase fluid displacement at the pore scale. Displacement efficiency is controlled by the coupled effects of fluid properties, pore structure, and wettability. While pore geometry is routinely characterized in dynamic core-flood experiments, quantitative assessment of wettability remains challenging. This limitation hampers the ability to evaluate wettability effects on flow behaviour, fluid trapping, and relative permeability (Kr).

In this study, wettability was systematically quantified by Amott–Harvey and USBM wettability indices (WI) and by advancing contact angles that were directly derived from capillary pressure (Pc) measurements. The influence of wettability on fluid trapping and endpoint relative permeability was investigated using carbonate and sandstone reservoir core samples. An initial dataset comprising dolomite and limestone samples was characterized using CT imaging, porosity–permeability measurements, petrographic analysis, and MICP. Porosity ranged from 0.15 to 0.31, and water permeability (Kw) spanned 1 to 500 mD. A second dataset of limestone and sandstone samples was analysed from Pc curves to further establish relationships between derived contact angles and dynamic imbibition behaviour.

Results revealed a strong correlation between wettability index values and advancing contact angles. Residual oil saturation (Sor) decreased with increasing advancing contact angle, whereas water relative permeability (Krw(Sor)) at residual oil saturation increased. Saturation changes during spontaneous displacement cycles were strongly governed by advancing contact angles: lower contact angles enhanced water imbibition, leading to increased oil trapping and higher Sor, while higher contact angles promoted oil spontaneous invasion, increased water trapping, and elevated residual water saturation (Swr) after secondary drainage. Distinct trends were observed between lithologies, indicating that dynamic displacement behaviour depends not only on wettability but also on pore geometry.

Across a wide experimental range (wettability index from +0.40 to −0.96 and advancing contact angles from 97° to 180°), wettability index values showed consistent agreement with contact angles derived from capillary pressure data. For the rock types studied, the results clearly define the impact of wettability and contact angle on endpoint properties and demonstrate that wettability behaviour varies with lithology and geological texture.

1 Introduction

Accurate knowledge of petrophysical and reservoir flow properties is essential for effective management and reliable forecasting of oil and gas reservoir performance. This requires a thorough understanding of the physical characteristics of reservoir rocks, the interactions between various fluids and pore surfaces, and the spatial distribution of pores and minerals within the porous medium.

Core laboratory data provides a solid foundation for reservoir modelling and formulation of efficient development strategies, including secondary recovery and enhanced oil recovery (EOR) methods [1].

Rock types are routinely characterized in experimental SCAL programs, but wettability is often poorly understood. This limitation restricts the ability to decouple and rigorously quantify the influence of wettability on dynamic fluid flow behaviour such as fluid trapping, endpoint saturation, capillary pressure and relative permeability. Hence, many of the laboratory-measured data remain unexplained because of poor wettability characterization.

Wettability can be characterized by contact angle measurements on mineral surfaces; however, such measurements are technically challenging and often yield highly unreliable results [2-4]. Furthermore, contact angle measurements may not be representative to actual

* Corresponding author: mdernaika@slb.com

reservoir rock as it is usually performed using smooth surfaces, hence ignoring the effect of roughness on contact angle [5]. Alternatively, wettability can be quantified using wettability index (WI) values derived from the Amott-USBM method, which is based on core-scale measurements of spontaneous imbibition and capillary pressure curves [6-9]. Nevertheless, these measurements are frequently not well correlated with endpoint fluid saturations and relative permeability data, and they are rarely obtained systematically across a wide range of rock types and lithologies.

There is a good understanding of the qualitative trends on how relative permeability and capillary pressure curves can vary as a function of wettability. However, the scatter in the data can be very large even within the same formation. The reason for the variation in the experimental measurements is related to the combined influence of wettability heterogeneity, pore geometry, saturation history, fluids and experimental uncertainties [10-12].

In this paper, we derived wettability index (WI) values from dolomite and limestone reservoir rock types (RRT) that underwent Amott-USBM wettability measurements. We studied variation of wettability as a function of rock type, and the impact of wettability on fluid trapping, Pc curve and endpoint Kr data. From the same set of samples, we derived advancing contact angles from the corresponding drainage-imbibition Pc curves based on the novel approach by Masalmeh and Jing [13], and we investigated potential relationship between WI and advancing contact angles.

On a different set of samples, we derived advancing contact angles for limestone and sandstone reservoir rocks that underwent primary drainage (PD) and imbibition Pc measurements. The aim was to further establish relationships between derived contact angles and dynamic imbibition behaviour.

Wettability was found to vary systematically with lithology and geological texture, exerting a clear influence on capillary pressure behaviour, fluid trapping, and endpoint properties. Wettability indices were consistent with the derived advancing contact angles, reinforcing their validity as quantitative indicators of wettability.

2 Fluid Displacement

2.1 Primary drainage

The primary drainage process occurs where the reservoir rock is typically strongly water wet. Consequently, primary drainage reflects water-wet behaviour characterized by low receding contact angles (i.e., <30°). Under these conditions, the initial water saturation (Swi) established at the end of primary drainage is largely independent of wettability that is usually established after oil migration to the reservoir, since oil—the non-wetting phase — invades water-filled/water-wet pores. The process is governed by pore-throat size distribution, whereby the non-wetting phase preferentially invades the largest available pore throats and progressively accesses smaller throats through invasion percolation [14].

2.2 Hysteresis and wettability changes

Fluid displacement is inherently hysteretic, reflecting irreversibility and path dependence. As a result, Pc curves depend not only on saturation but also on the saturation path (drainage or imbibition) and saturation history. The main contributors to hysteresis are contact angle hysteresis, fluid trapping, and wettability [15].

Contact angle hysteresis refers to the dependence of the contact angle on the direction of displacement. The receding contact angle during drainage is consistently smaller than the advancing contact angle during imbibition. This difference is commonly attributed to surface roughness, chemical heterogeneity, contamination, and non-equilibrium effects at the fluid-solid interface [16,17].

Fluid trapping arises from pore-space geometry and instabilities in fluid-fluid interface configurations. During primary drainage, instability occurs when an advancing interface experiences a reduction in curvature, leading to rapid displacement events known as Haines jumps [18]. These jumps are irreversible and contribute significantly to hysteresis between drainage and imbibition cycles. Their occurrence is enhanced in pore systems with large pore-body-to-pore-throat aspect ratios, which directly influence the magnitude of hysteresis loops [19].

Wettability describes the preference of a rock surface for one fluid over another [20] and plays a central role in determining residual oil saturation, as well as capillary pressure and relative permeability behavior [21,22]. During primary drainage, a thin water film typically remains adsorbed on the pore surface, shielding the rock from direct contact with oil. As capillary pressure increases, a critical threshold may be reached at which this water film becomes unstable and ruptures, allowing oil to contact the solid surface. The stability of this film is controlled by the balance between capillary pressure and the disjoining pressure isotherm [23], which depends on mineralogy, fluid composition, and pore geometry. Once oil contacts the surface, wettability alteration may occur depending on the strength of the rock-fluid interactions. However, water often remains in pore corners and crevices, preserving locally water-wet conditions. This leads to mixed-wet systems characterized by spatial heterogeneity in wettability [24].

Wettability alteration, particularly through the loss of protective water films, can significantly enhance contact angle hysteresis [18]. While wettability alteration and contact angle hysteresis originate at the pore scale, fluid trapping occurs at a larger scale and is primarily controlled by pore morphology. Together, these processes strongly influence the extent of trapping and the overall hysteretic behaviour of capillary pressure curves.

2.3 Water spontaneous imbibition

During water spontaneous imbibition (SI), water re-enters oil-filled pores that remain water-wet as capillary pressure decreases from its maximum value toward zero. This process occurs under positive capillary pressure, where the oil phase pressure exceeds that of water.

Water preferentially invades the smallest pore throats first, in contrast to primary drainage. The displacement is governed by pore-body filling rather than pore-throat entry. The dominant pore-scale mechanism is snap-off, which occurs in pore throats and leads to the trapping of oil as disconnected ganglia within pore bodies.

The extent of oil trapping is strongly influenced by interface curvature, which depends on the advancing contact angle and pore geometry. It is also affected by the water saturation at maximum capillary pressure. Snap-off efficiency is closely related to the pore-throat-to-pore-body aspect ratio [25], with higher aspect ratios favouring increased trapping.

2.4 Forced imbibition

If the rock remains strongly water-wet and no wettability alteration occurs during primary drainage, then imbibition is entirely spontaneous, and no forced imbibition is observed. However, if wettability alteration leads to non-water-wet conditions in portions of the pore space, forced imbibition becomes significant. In such cases, water invades the non-water-wet pores under negative capillary pressure. The invasion proceeds from larger to smaller pores and is characterized by piston-like displacement, with minimal snap-off and limited oil trapping at the pore scale. In the limiting case where all pores become non-water-wet, the forced imbibition Pc curve approaches the mirror image of the primary drainage curve [15,24].

2.5 Spontaneous drainage

During spontaneous drainage (SpD), oil re-enters water-filled pores that are non-water-wet as capillary pressure decreases from its maximum negative value toward zero. Oil preferentially invades the smallest pore throats first. The displacement is governed by pore-body filling rather than pore-throat entry. The dominant pore-scale mechanism is snap-off, which occurs in pore throats and leads to the trapping of water as disconnected ganglia within pore bodies.

2.6 Secondary drainage

Secondary drainage (SD) refers to the re-invasion of oil into the rock following spontaneous drainage cycle. Unlike primary drainage, this process occurs in a system where wettability may have been altered. Oil invasion during secondary drainage is influenced by contact angle hysteresis, resulting in lower positive entry pressures compared to primary drainage. The oil invasion can happen in water-wet and non-water-wet pores (which were not invaded during SpD) with receding contact angles higher than 30° but lower than 90°. Water trapping may occur in the non-water-wet pores. Due to water trapping (in SpD and SD), an increase in residual water saturation (Swr) at the end of the secondary drainage process is expected (e.g., [15]).

3 Core Material

Core plug samples (1.5-inch diameter) were collected from several reservoirs in the Middle East. The first set of plugs (Reservoirs 1-3) consisted of dolomite and limestone samples, which were subjected to Amott-USBM wettability tests. The second set (Reservoirs 4-5) comprised mainly sandstone, along with one limestone sample, and underwent primary drainage and imbibition Pc measurements. Figure 1 shows the distribution of porosity-permeability characteristics for all samples. The figure legend identifies each sample's lithology, test type, and reservoir of origin.

Figures 2-6 present the rock type (RRT) classification for all samples from Reservoirs 1-5. The RRTs are defined based on an integration of petrophysical properties and geological textures. Textural characteristics were determined from thin-section photomicrographs, while petrophysical properties were derived from mercury injection Pc capillary pressure curves and pore-throat size distribution (PTSD). The MICP plots include sample ID, helium porosity, and water permeability (Kw) in their respective legends. Similarly, the thin-section photomicrographs provide sample ID along with corresponding porosity, permeability, and texture classification. Capillary pressure curves were converted from mercury-air system to oil-water system using measured interfacial tension (IFT) of the oil-water fluid pair, and an IFT value of 485 mN/m for the mercury-air system [2]. Following the recommendations of Masalmeh and Jing [1,13], the conversion assumes identical contact angles for both fluid systems; therefore, only the ratio of interfacial tensions was applied in the transformation. A summary of the RRT classifications and associated properties is provided in Table 1.

It is not the purpose of this study to provide detailed descriptions of the identified RRTs. The reader is referred to our previous research studies on rock typing (e.g., [26]) or to well-documented rock typing publications (e.g., [27-29]) for further insight into the classification and characteristics of various rock types.

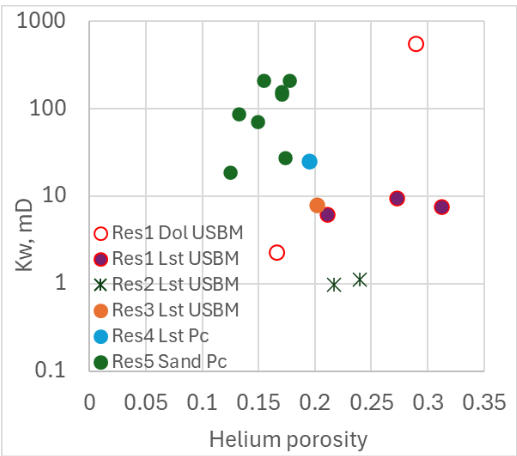

Fig. 1. Porosity-permeability characteristics for all samples

It should be noted; however, that a strong link is observed across all samples between permeability, capillary entry pressure, and pore-throat size. As permeability increases, pore-throat sizes become larger, while capillary entry pressure decreases.

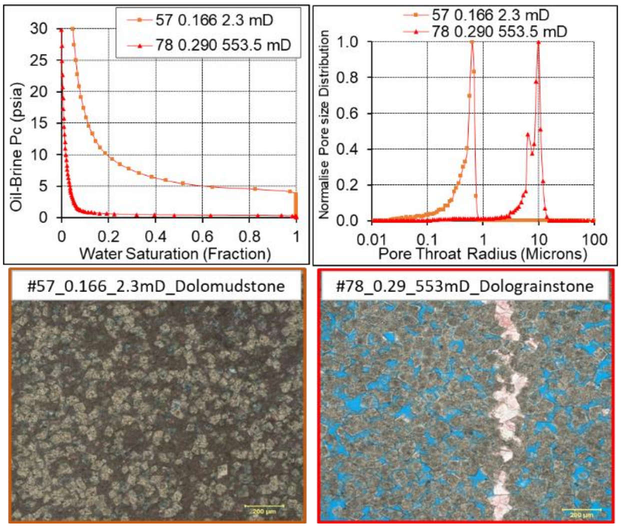

Fig. 2. Dolomite RRTs (Reservoir 1)

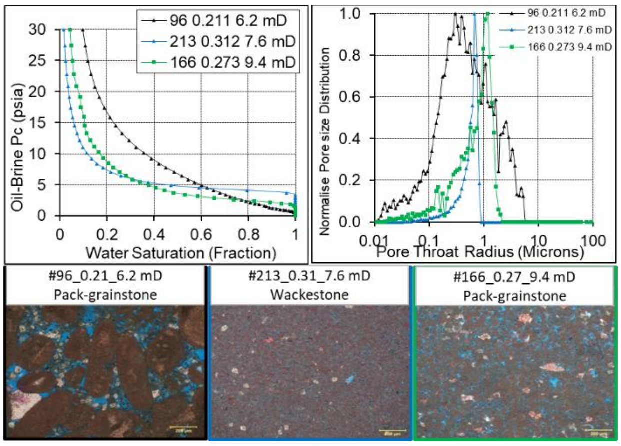

Fig. 3. Limestone RRTs (Reservoir 1)

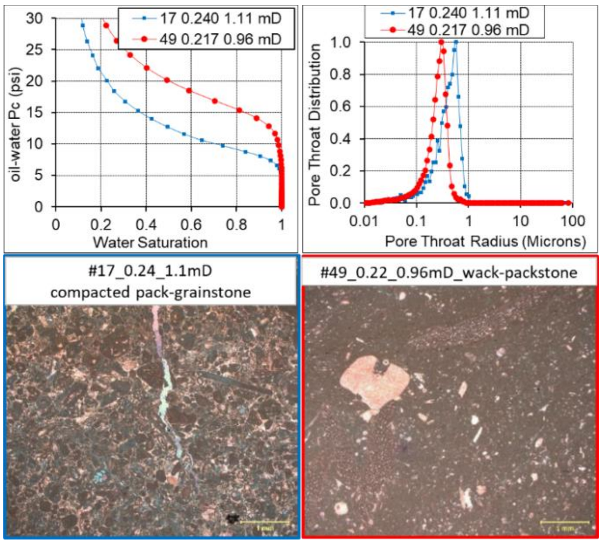

Fig. 4. Limestone RRTs (Reservoir 2)

Samples from Reservoirs 1-3 were solvent-cleaned at high temperature using a flow-through technique with repeated cycles of toluene, chloroform and methanol. The samples were then oven-dried to constant weight before measurements of helium porosity and gas permeability were performed. Subsequently, the samples were saturated with synthetic formation water to determine Kw.

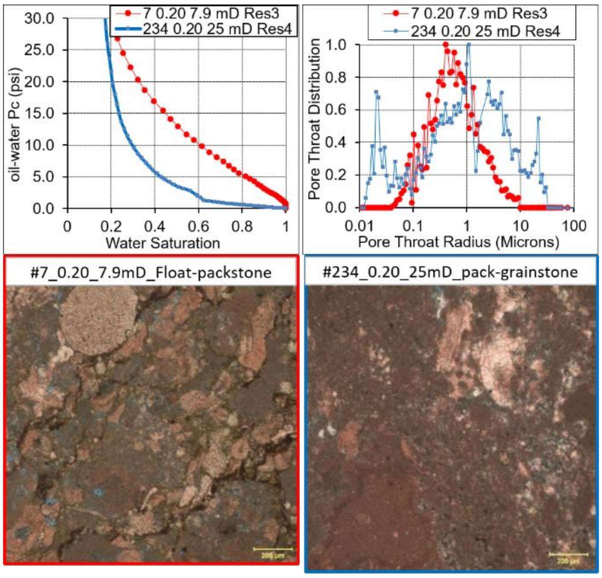

Fig. 5. Limestone RRTs (Reservoir 3 &4)

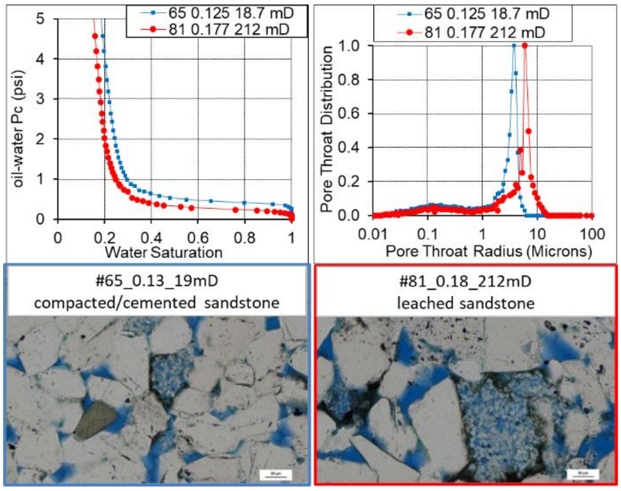

Fig. 6. Representative sandstone RRTs (Reservoir 5)

Table 1. Summary of RRT information for all samples.

Reservoir	Lithology	Texture	PTSD	Test	Porosity	Kw (mD)
Res1	Dol	mudstone	uniform	USBM	0.17	2.3
Res1	Dol	grainstone	uniform	USBM	0.29	553
Res1	Lst	wackstone	uniform	USBM	0.31	7.6
Res1	Lst	pack-grainstone	uniform	USBM	0.27	9.4
Res1	Lst	pack-grainstone	wide	USBM	0.21	6.2
Res2	Lst	wack-pack-grainstone	uniform	USBM	0.22-0.24	0.96-1.1
Res3	Lst	Float-packstone	wide	USBM	0.20	7.9
Res4	Lst	pack-grainstone	wide	Pc	0.20	25
Res5	Lst	sandstone	uniform	Pc	0.13-0.18	20-200

4 Amott-USBM Wettability Tests

The plugs underwent multi-speed gas-water centrifugation (with a maximum rotational speed of 10,000 RPM) to obtain accurate primary drainage Pc curve down to Swi, eliminating the influence of any residual non-water wet conditions caused by potentially incomplete solvent cleaning (see the impact of inefficient cleaning on PD oil-water Pc in [13]. Fluid production stability at each rotational speed was ensured using an automated data acquisition system. The PD air-water Pc was converted to oil-water Pc by using the Laplace Pc relationship and the respective IFT values [1,13,30]. In this study, the gas-water IFT was taken as 72 dynes/cm [31], while the oil-water IFT was measured under experimental conditions to obtain accurate oil-water Pc curve. Inaccurate PD Pc will have a direct impact on the derivation of the advancing contact angle. The Swi values ranged from 0.031 to 0.125. Lower porosity samples tend to show higher Swi values. The samples were flooded with Isopar-L mineral oil to replace air under high pore pressure and then aged in crude oil at reservoir temperature for 4 weeks. Effective oil permeability (Ko(Swi)) was measured at Swi, and the samples gave reasonably high relative permeability to oil (Kro(Swi)), which mainly varied from 0.70 to 0.90. The Kr values were calculated using Kw as the base permeability.

Water spontaneous imbibition (SI) was conducted using an Amott cell, while forced imbibition (FI) was performed in a high-speed centrifuge, where the samples were spun under water at multiple rotational speeds until residual oil saturation (Sor) was reached. All samples were subjected to a maximum rotational speed of 6,500 rpm, except for those with high permeability and uniform pore throat size distribution (PTSD), which were tested at a maximum speed of 3,000 RPM. The samples showed an increase in water SI that ranged from 0.013Sw to 0.34Sw. Upon the multi-speed water-oil imbibition centrifugation, the samples gave average Sor values that ranged from around 0.10 to 0.20. Sor tends to be higher in samples that exhibit greater water SI. Kw measurements were performed at Sor and gave Krw(Sor) that ranged from 0.31 to 0.79. Krw(Sor) tends to increase as Sor decreases. The samples were then placed in Amott cell under oil, where they exhibited spontaneous oil invasion that varied among the samples, ranging from approximately 0.02 to 0.55. The dolomite samples showed a significantly higher degree of spontaneous oil invasion (0.33 – 0.55), whereas the limestone samples exhibited lower values (0.02 – 0.37).

Secondary drainage (SD) was performed in the high-speed centrifuge where the samples were spun under oil at multiple speeds down to residual water saturation (Swr). The samples gave Swr values that ranged from 0.14 to 0.42 (all Swr values were higher than Swi after primary drainage). Swr is higher in samples that exhibit greater SpD due to larger water trapping as water trapping increases with increasing oil-wetness [15]. Oil permeability measurements were performed at Swr and gave Kro(Swr) that ranged from 0.33 to 0.68. All Kro(Swr) were lower than Kro(Swi).

The capillary pressure (Pc) curves were calculated using the Hassler–Brunner Pc and Forbes Pc solutions [47,48]. Both methods produced comparable Pc curves by transforming average saturation data (derived from production measurements) and rotational speed data into a Pc–Sw curve at the inlet face of the sample. All saturation values reported in this study represent average saturations calculated from the experimental production data and the sample pore volume. Wettability Index (WI) values were calculated using Amott index, Amott-Harvey Index and USBM Index including bounded USBM [6,7,32]. The bounded USBM index can be useful in cases where the USBM index varies beyond the range of -1 to +1 as highlighted by Mirzaei-Paiaman [32]. In this study, consistent wettability indices were obtained using Amott-Harvey (AH), USBM, and bounded USBM. The AH WI values ranged from +0.40 to −0.96.

Advancing contact angle was derived based on a novel procedure as described in [13]. The procedure allows for the derivation of imbibition capillary pressure from primary drainage Pc considering wettability and fluid trapping. The derivation is based on a conceptual model in oil wet and mixed wet systems where imbibition Pc curve is the mirror-image of the primary drainage Pc curve. This condition can only be true for systems showing no (or little) spontaneous water imbibition, and hence the procedure may not be applied when the sample shows high water spontaneous imbibition. For the samples studied, the derived advancing contact angles were in the range of 97° to 180°.

Figure 7 presents representative results from the Amott-USBM wettability measurements for Reservoir 1. Figure 7a illustrates a strongly oil-wet dolomite (500 mD), characterized by an Amott-Harvey index (I_{AH}) of -0.96 and an advancing contact angle (θa) of 180°. Figure 7b shows an intermediate-wet (slightly oil-wet) limestone (6.2 mD), with I_{AH} of 0.13 and θa of 105°. The legend in each plot identifies the sequential stages of wettability measurements, including PD Pc, water SI, FI, SpD, and SD. It also indicates the derived θa value associated with the solid (FI negative Pc) curve. This curve was obtained by transforming the oil-water PD Pc curve through adjustment of the advancing contact angle to match the experimentally measured imbibition Pc data [13]. As shown in Figure 7, there is very good agreement between the measured FI data points and the calculated imbibition Pc curve, thereby validating the derived advancing contact angle for imbibition. The plots also give water index (Iw), oil index (Io), I_{AH}, USBM index, bounded USBM index and wettability state.

For the samples from Reservoirs 1-3, the calculated WI spans water-wet, intermediate-wet (i.e., slightly water-wet, neutral, and slightly oil-wet), and oil-wet conditions. Figure 8 shows the wettability states of the samples, classified using cut-off values of -0.3, -0.1, +0.1, and +0.3, following the criteria of Cuiec [33]. This classification may appear ambiguous because two samples with positive WI values, interpreted as neutral to slightly water-wet, also exhibit advancing contact angles greater than 90°.

A good correlation is observed between the WI values and the derived contact angles for negative WI values. A deviation from linearity ($\theta a = 90*(1\text{-}WI)$) is observed for positive WI values. This behavior is expected as the procedure to determine the contact angle is less accurate with increasing spontaneous imbibition. Moreover, in this range the wettability index calculation is most affected by contact angle hysteresis and may not be representative. These samples, which fall within the neutral and slightly water-wet regime, exhibited water SI of 0.085Sw and 0.149Sw, respectively.

The advancing contact angle was not determined for one limestone sample #213 from Reservoir 1 (see figure 3), as it exhibited significant water SI of 0.34 Sw (in addition to FI), resulting in a WI of +0.40. This sample is characterized by a homogeneous wackstone texture, with porosity of 0.31 and Kw of 7.6 mD. For such a system, a distribution of contact angles would be expected, reflecting water invasion occurring during both SI and FI.

Figure 9 demonstrates generally good agreement between the USBM index and the AH WI. However, one sample classified as water-wet based on a high AH WI value (+0.40) appears nearly neutral when evaluated using the USBM index.

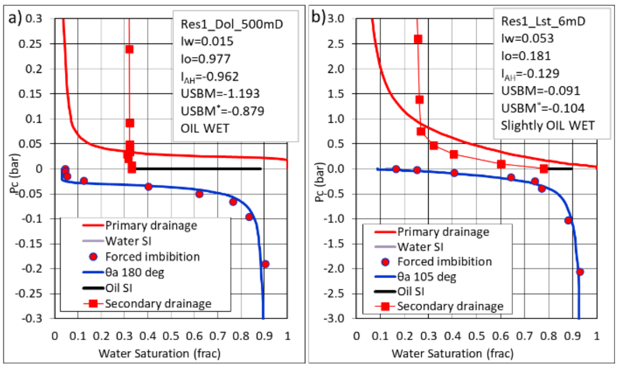

Fig. 7. Example Amott-USBM wettability results from a) an oil-wet dolomite showing advancing contact angle 180 degrees and b) an intermediate-wet (slightly oil-wet) limestone showing advancing contact angle 105 degrees (Reservoir 1).

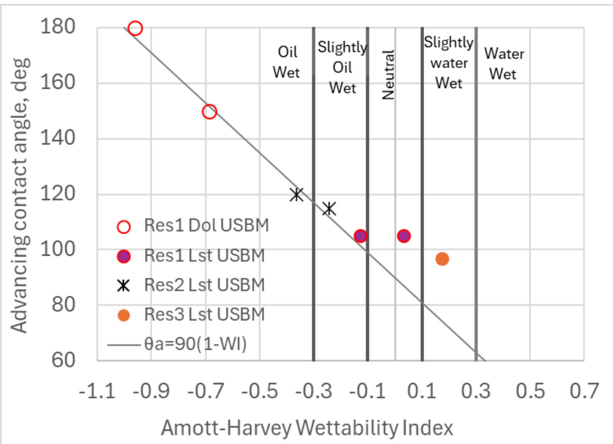

Fig. 8. Relation between WI and advancing contact angle.

5 Drainage-Imbibition Pc Measurements

Samples from Reservoirs 4-5 followed the same primary drainage and imbibition multi-speed centrifuge procedures described earlier. Sample preparation and characterization, including solvent cleaning, oven drying, and measurements of helium porosity and gas permeability, were conducted in accordance with the procedures described for samples from Reservoirs 1–3. However, the sandstone samples from Reservoir 5 were not subjected to spontaneous imbibition in the Amott cell. For the sandstone samples, irreducible water saturation (Swi) ranged from 0.10 to 0.23, with lower-porosity samples generally exhibiting higher Swi values. The samples showed relatively high Kro(Swi), varying between 0.64 and 0.88. Following multi-speed water-oil imbibition centrifugation, Sor ranged from 0.15 to 0.39. Krw(Sor) ranged from 0.17 to 0.72 and tended to increase as Sor decreased. Advancing contact angles for the sandstone samples, derived from the measured drainage-imbibition Pc data, ranged from 100° to 121°.

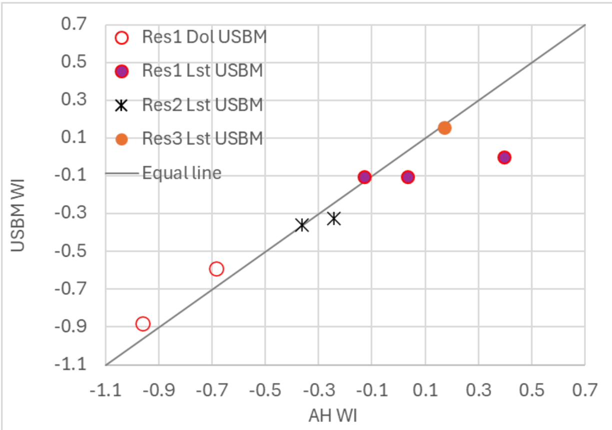

Fig. 9. USBM WI vs AH WI

6 Results and Discussions

Figure 10a shows a strong correlation between Swi and porosity across all samples. This relationship is well established in the literature [e.g., 34,35] and suggests that the data quality for the studied reservoirs is high. It is worth noting that such a correlation may not be reliably observed when Swi values are obtained from core flooding experiments [36]. In contrast, Figure 10b indicates that Swi exhibits little to no dependence on permeability [13,49].

Figure 11 illustrates the variation of Sor with both porosity and permeability. The carbonate RRTs do not display any significant relationship between Sor and porosity or permeability. However, the sandstone samples show a distinct trend compared to carbonate samples, which may be attributed to differences in pore geometry.

Figure 12 illustrates the variation of endpoint Kro and Krw with permeability. The Kro(Swi) values predominantly range between 0.60 and 0.90 and do not exhibit any clear correlation with permeability. Similarly, Krw(Sor) shows no significant dependence on permeability. Although there may appear to be a potential correlation between Krw(Sor) and permeability for the sandstone samples, this trend is not consistent. Specifically, several samples with similar permeability values (around 100 mD) display a wide variation in Krw(Sor), ranging from 0.30 to 0.70. Therefore, no reliable correlation can be established from this dataset.

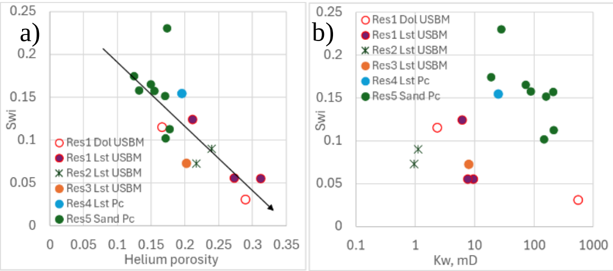

Fig. 10. Change of Swi with porosity and Kw

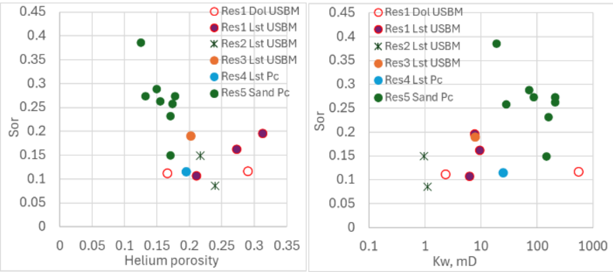

Fig. 11. Change of Sor with porosity and Kw

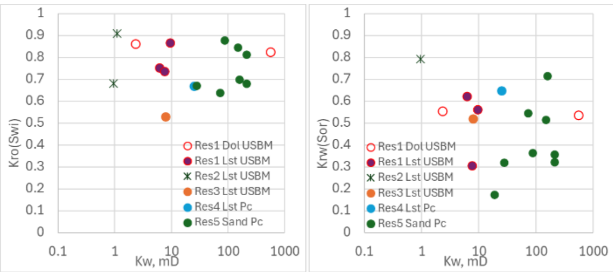

Fig. 12. Change of endpoint Kro and Krw with Kw

Figure 13a examines any possible variation of wettability with permeability for the USBM samples, while Figure 13b presents variation of contact angles with permeability for all reservoir samples under study. As shown in Figure 13a, the dolomite samples from Reservoir 1 exhibit strongly oil-wet conditions, with WI values lower than −0.60. In contrast, limestone samples from Reservoir 2 indicate slightly oil-wet conditions, with an average WI of approximately −0.3. Meanwhile, limestone samples from Reservoirs 1 and 3 display nearly neutral to slightly water-wet behavior, with WI values ranging from −0.1 to +0.4.

Although the dataset is insufficient to establish a definitive relationship between wettability and rock type, the results suggest that wettability varies with both lithology and reservoir (i.e., fluid properties). Wettability is governed by complex rock-fluid interactions, which are influenced by factors such as fluid composition, mineralogy, surface roughness, temperature, pressure, and the thickness of water films [23].

Figure 13b further confirms the wettability conditions of samples from Reservoirs 1-3 based on the corresponding advancing contact angles. In addition, the single limestone sample from Reservoir 4 exhibits slightly oil-wet behavior, with a contact angle of 110°. The sandstone samples from Reservoir 5 display an intermediate wettability with slightly oil wet conditions with contact angles varying from 108° to 121°.

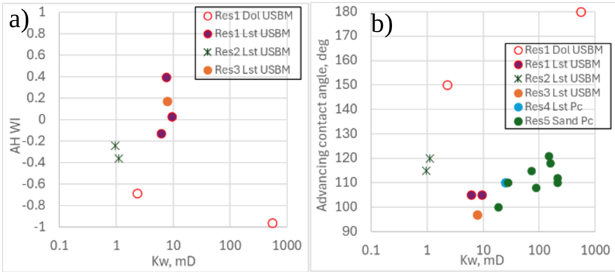

Fig. 13. Variation of WI and contact angles with Kw

Table 2 summarizes wettability index (WI) and corresponding derived contact angles for all samples. Similar wettability conditions are highlighted using consistent color coding based on Table 3. Table 3 presents relationship between wettability classes and WI values (after Cuiec [33]), along with an attempt to correlate the derived advancing contact angles with wettability behavior based on the dataset of this study.

Wettability results should be interpreted with caution and may require additional contextual discussion [33]. For instance, the limestone sample from Reservoir 1 (Sample #213, wackstone texture), with a WI of +0.4, is classified as water-wet. Nevertheless, its actual wettability is heterogeneous in nature, with a water index of 0.46 and an oil index of 0.06. The sample exhibited both spontaneous and forced water imbibition values of 0.34 and 0.41, respectively. Its positive WI is primarily attributed to the limited spontaneous oil invasion, where the spontaneous drainage and secondary drainage values were 0.04 and 0.62, respectively.

Figure 14 illustrates the variation of contact angles with grain density (i.e., lithology). Both limestone and sandstone samples exhibit a similar range of contact angles, predominantly between 100° and 120°, indicating neutral to slightly oil-wet conditions. In contrast, the two dolomite samples from Reservoir 1 display significantly higher contact angles, ranging from 150° to 180°, corresponding to strongly oil-wet conditions. These observations highlight the pronounced influence of lithology on wettability behavior. This is indeed in line with previous research that dolomite frequently exhibits more oil wet behavior than limestone in comparable environments due to differences in surface reactivity and mineral composition [37-40].

Figure 15 presents variation of endpoint Kro(Swi) and Krw(Sor). Although Swi varies over a wide range (0.03-0.23), it does not exhibit a significant impact on Kro(Swi). While a decreasing trend of Kro(Swi) with increasing Swi might be expected, such behavior is typically observed within similar rock types [41,42].

In contrast, a clear decreasing trend of Krw(Sor) with increasing Sor is observed, indicating a strong influence of residual oil saturation on endpoint Krw(Sor). The scatter of data points around the Krw(Sor) trend is attributed to variations in wettability among the samples. For example, the lower data point corresponds to the water-wet sample #213 (WI = +0.4), where stronger water-wet conditions result in lower Krw, as expected [15,43]. Conversely, the upper scatter is associated with samples exhibiting higher contact angles, which lead to higher Krw(Sor) at comparable Sor. It is anticipated that the Krw(Sor) relationship would show improved alignment if plotted against contact angle rather than Sor alone.

6.1 Effect of wettability on endpoint properties

It has been experimentally observed that oil-wet to mixed-wet conditions lead to higher endpoint Krw(Sor) and lower Sor, compared to water-wet conditions [15,43-45]. The variation of these endpoint properties with wettability has also been explained using a conceptual model by Masalmeh [15]. More recently, trends in Krw(Sor) and Sor as a function of contact angle have been investigated using pore-scale simulations in a single digitized rock sample [46]. However, to the best of our knowledge, none of these studies have provided a rigorous experimental quantification of the magnitude of endpoint property variation associated with wettability alteration.

Table 2. Summary of the WI and contact angles.

	Lithology	Texture	PTSD	WI	Contact angle (°)	Wettability condition
Res1	Dol	mudstone	uniform	-0.69	150	strongly oil wet
Res1	Dol	grainstone	uniform	-0.96	180	strongly oil wet
Res1	Lst	wackstone	uniform	+0.4	-	water wet
Res1	Lst	pack-grainstone	uniform	+0.03	105	Intermediate wet (neutral)
Res1	Lst	pack-grainstone	wide	-0.1	105	Intermediate wet (neutral)
Res2	Lst	wack-pack-grainstone	uniform	(-0.36) - (-0.24)	115-120	Intermediate wet (slightly oil wet)
Res3	Lst	Float-packstone	wide	+0.2	97	Intermediate wet (slightly water wet)
Res4	Lst	pack-grainstone	wide	-	110	Intermediate wet (slightly oil wet)
Res5	Lst	sandstone	uniform	-	108 - 121	Intermediate wet (slightly oil wet)

Table 3. Potential relation between wettability class, wettability index and advancing contact angle.

	oil wet	Intermediate wet				water wet	
		slightly oil wet	Neutral		slightly water wet		
WI	-1	-0.3	-0.1	0	+0.1	+0.3	+1
θa °	> 125	125 - 110	110 - 105	105 - 100	100 - 90	< 90	

Figure 16 shows variation of endpoint Krw(Sor) and Sor as a function of the AH WI. The dataset comprises dolomite and limestone samples from Reservoirs 1-3. For the limestone samples, over a WI range of −0.4 to +0.4, Krw(Sor) decreases from approximately 0.8 to 0.3, while Sor increases from about 0.09 to 0.20. In contrast, the dolomite samples exhibit a different trend, with WI values ranging from −0.69 to −0.96, Sor values of approximately 0.10, and Krw(Sor) of around 0.55. However, due to the limited number of dolomite samples, no definitive trend can be established for this lithology.

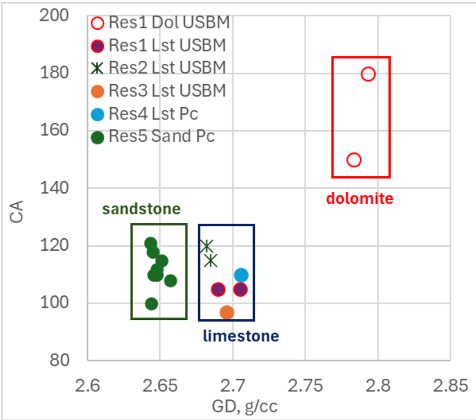

Fig. 14. Variation of CA with GD

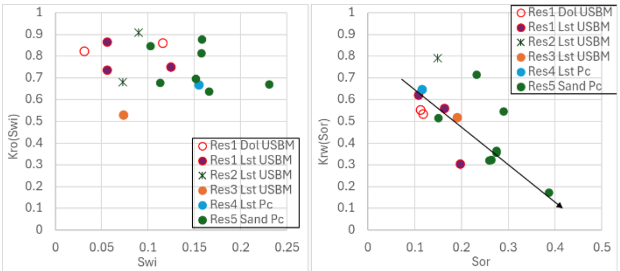

Fig. 15. Variation of endpoint Kro and Krw with saturation

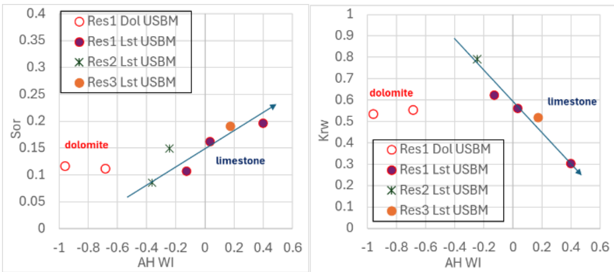

Fig. 16. Variation of endpoint Sor and Krw with WI

Figure 17 illustrates that Swi is not a function of wettability. This is because primary drainage (oil invasion) occurs in initially water-wet pores, while wettability alteration takes place after oil has invaded the pore space. Therefore, Swi is expected to be largely independent of wettability that is measured after oil invasion. The figure also indicates that Kro(Swi) is not a strong function of wettability as the fluid distribution is determined at the end of primary drainage, which is performed under water-wet conditions. While wettability changes during aging, however, the fluid distribution does not change to reflect such wettability alteration and its effect on the oil end point may not be significant.

Figure 18 presents variation of Krw(Sor) and Sor as a function of contact angle for all samples, comprising three lithologies: dolomite, limestone, and sandstone. The figure demonstrates a strong dependence of these trends on lithology. Distinct behaviors are observed for each lithology, with Krw(Sor) increasing and Sor decreasing as the contact angle increases (i.e., toward more oil-wet conditions).

Due to the limited number of samples, no definitive trend can be established for the dolomite dataset. For the limestone samples, over a contact angle range of 97° to 120°, Krw(Sor) increases from approximately 0.5 to 0.8, while Sor decreases from about 0.20 to 0.09. For the sandstone samples, over a similar contact angle range, Krw(Sor) increases from approximately 0.2 to 0.7, while Sor decreases from about 0.40 to 0.15.

Table 4 provides endpoint properties (i.e., Sor and Krw) with varying wettability conditions.

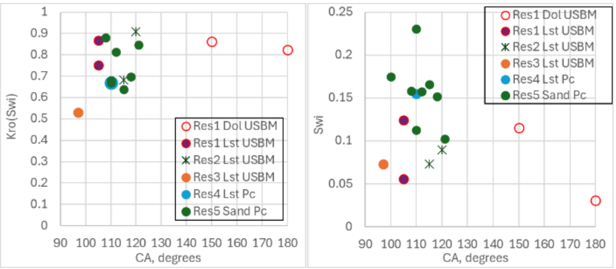

Fig. 17. Variation of endpoint Swi and Kro with WI.

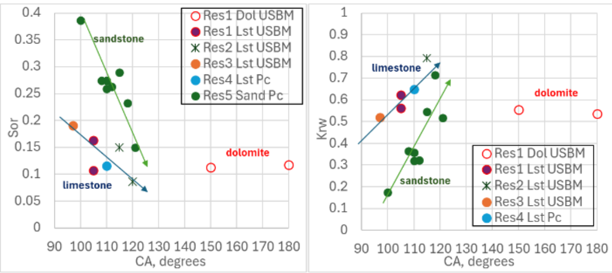

Fig. 18. Variation of endpoint Sor and Krw(Sor) with CA

Table 4. Endpoint properties with varying wettability conditions

	Lithology	WI	θa °	Wettability condition	Sor	Krw(Sor)
Res1	Dol	-0.69	150	strongly oil wet	0.11	0.55
Res1	Dol	-0.96	180	strongly oil wet	0.12	0.54
Res1	Lst	+0.4	-	water wet	0.20	0.31
Res1	Lst	+0.03	105	Intermediate wet (neutral)	0.16	0.56
Res1	Lst	-0.1	105	Intermediate wet (neutral)	0.11	0.62
Res2	Lst	(-0.36) - (-0.24)	115-120	Intermediate wet (slightly oil wet)	0.15	0.79
Res3	Lst	+0.2	97	Intermediate wet (slightly water wet)	0.19	0.52
Res4	Lst	-	110	Intermediate wet (slightly oil wet)	0.12	0.65
Res5	Lst	-	108 - 121	Intermediate wet (slightly oil wet)	0.15 - 0.39	0.17 - 0.52

6.2 Effect of wettability on fluid trapping

Figure 19a illustrates the increase in water spontaneous imbibition (SI) as the system becomes less oil wet. This dataset provides direct evidence of water SI occurring in mixed-wet carbonate systems. In this study, the maximum saturation change during water SI reached approximately 0.35 (for sample #213). Water SI becomes significant when the WI exceeds +0.1 (corresponding to contact angles below 100°). Figure 19b shows that Sor increases with increasing water SI, hence increasing water-wetness.

Figure 20a establishes a direct relationship between advancing contact angle and spontaneous drainage. Higher advancing contact angles during imbibition promote greater spontaneous drainage. The figure shows an approximately linear correlation, with SpD increasing from nearly zero to about 0.55 as the advancing contact angle increases from 97° to 180°. Figure 20b demonstrates the impact of SpD on the endpoint residual water saturation (Swr) at the end of secondary drainage. Increased SpD leads to greater water trapping, resulting in higher Swr.

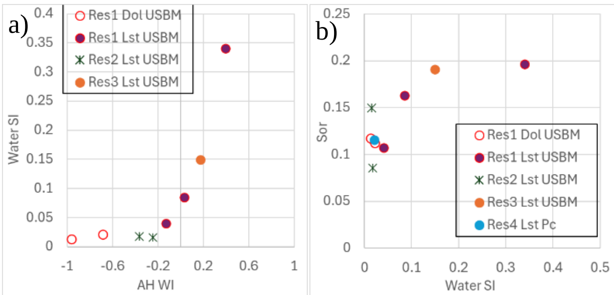

Fig. 19. Variation of water SI with WI and its impact on Sor

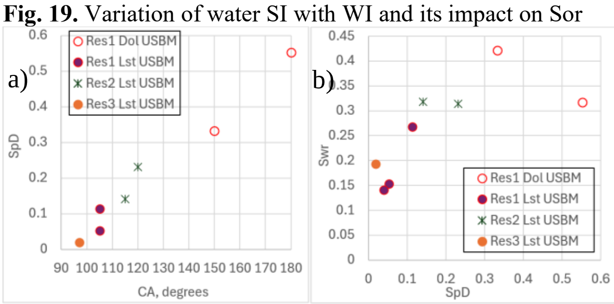

Fig. 20. Variation of SpD with CA and its impact on Swr

6.3 Effect of wettability on the Pc shape

Figure 7 provided an example of how Pc curves vary under different wettability conditions. Both the dolomite (oil-wet) and limestone (intermediate-wet) samples showed that the measured imbibition Pc curves are approximately the mirror image of the primary drainage Pc curves. This symmetry allows derivation of advancing contact angles using the Masalmeh model [13]. Due to the contrasting wettability states between the two samples and the large difference in advancing contact angles (180° versus 105°), the samples exhibit distinctly different secondary drainage behavior. In this perspective, figure 21 presents the Pc cycles for the water-wet sample #213. This sample exhibits a significantly different imbibition Pc curve, consistent with strong water SI effects. In this case, the advancing contact angle could not be reliably derived using the proposed model. Strictly speaking, the pore system invaded during water spontaneous imbibition is expected to correspond to pores with effective contact angles below 90°, whereas the pores accessed during forced imbibition are expected to be associated with effective contact angles above 90°.

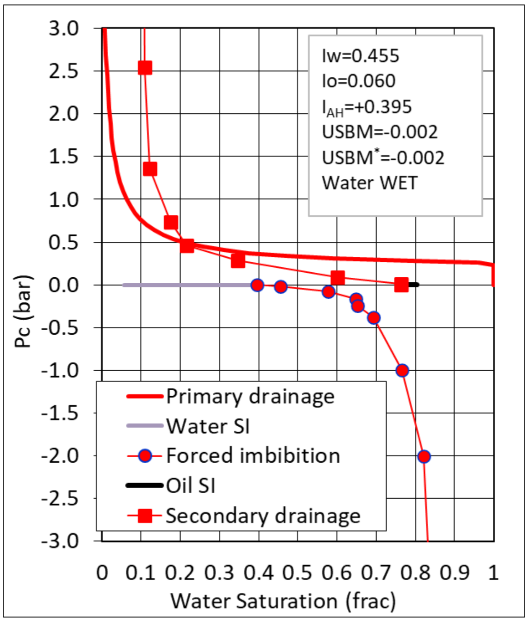

Fig. 21. Amott-USBM wettability results from the water-wet limestone sample showing AH WI of +0.4. (Reservoir 1).

7 Summary and Conclusions

Rock wettability was characterized by two methods: Wettability Index values from Amott-USBM measurements and advancing contact angles derived from primary drainage and imbibition Pc curves. The influence of wettability on fluid trapping and endpoint relative permeability was investigated using carbonate and sandstone reservoir core samples. The following conclusions are drawn from this study.

1. Consistent wettability indices were obtained using Amott-Harvey, USBM, and bounded USBM methods, confirming the reliability of these approaches for wettability characterization.
2. A strong correlation was established between wettability index values and advancing contact angles, validating the use of contact angle as a representative wettability indicator.
3. Wettability was reliably quantified by the Masalmeh model using drainage-imbibition Pc curves (without SpD and SD), significantly reducing experimental turnaround time for wettability programs.
4. A clear inverse relationship was observed between initial water saturation (Swi) and porosity, with Swi decreasing as porosity increases across all samples.
5. No systematic correlation was identified between fluid trapping or relative permeability endpoints and the porosity-permeability characteristics of the samples.
6. Both limestone and sandstone lithologies exhibited a similar range of advancing contact angles (100°-120°), however, they demonstrated distinct dynamic displacement behaviours, attributed to differences in pore geometry and structure.
7. Dolomite samples showed significantly higher contact angles (150°-180°), corresponding to strongly oil-wet conditions, highlighting the pronounced influence of lithology on wettability.
8. Residual oil saturation (Sor) decreased with increasing advancing contact angle, while water relative permeability at Sor (Krw(Sor)) increased.
9. Higher contact angles promoted spontaneous drainage, leading to increased water trapping and elevated residual water saturation following secondary drainage.
10. Our proposed approach provides the opportunity to determine reliable wettability parameters in the form of direct contact angle inputs for pore-scale numerical modelling studies.

Nomenclature

Symbol

Kl	Klinkenberg permeability
Kr	Relative permeability
Kro	Oil relative permeability
Krw	water relative permeability
Kw	Water permeability
Pc	Capillary pressure
Sw	Water saturation
Swi	Initial water saturation
Swr	Residual water saturation
Sor	Residual oil saturation
θa	Advancing contact angle
WI	Wettability Index
I	Index
I_{AH}	Amott-Harvey Index
Iw	Water Index
Io	Oil Index

Abbreviations

AH	Amott-Harvey
CA	Contact Angle
CT	Computed Tomography
deg	Degrees
EOR	Enhanced Oil Recovery
GD	Grain Density
Imb	Imbibition
MICP	Mercury Injection Capillary Pressure
PD	Primary Drainage
RCA	Routine Core Analysis
RPM	Rounds Per Minute
RRT	Reservoir Rock Type
SCAL	Special core analysis
SI	Spontaneous Imbibition
SD	Secondary Drainage
SpD	Spontaneous Drainage
USBM	United States Bureau of Mines
°	Degrees
%	Percent

The authors would like to acknowledge ADNOC and SLB Management for the permission to publish the results of this study. Special thanks to Ibrahim Shalby and Teslisporo Lacaba from SLB Abu Dhabi Laboratory for careful experimental measurements and calculations.

References

1. S.K. Masalmeh, and X.D. Jing, The Importance of Special Core Analysis in Modelling Remaining Oil Saturation in Carbonate Fields, SCA-2008-03 (2008)
2. Morrow, N.R. and Melrose, J.C.: "Application of Capillary Pressure Measurements to the Determination of Connate

Water Saturation", Interfacial Phenomena in Petroleum Recovery, N.R. Morrow (ed.), Marcel Dekker, New York City (1991) 257-287.

3. Iglauer, S. Salamah, A. Sarmadivaleh, M. Liu, K. and Phan, C. (2014). Contamination of silica surfaces: Impact on water-CO2-quartz and glass contact angle measurements. International Journal of Greenhouse Gas Control. 22: pp. 325-328.
4. Chau, T.T. (2009) A review of techniques for measurement of contact angles and their applicability on mineral surfaces, Minerals Engineering, Volume 22, Issue 3, 2009, Pages 213-219, ISSN 0892-6875, https://doi.org/10.1016/j.mineng.2008.07.009.
5. AlRatrout, A., Blunt, M. J., & Bijeljic, B. (2018). Wettability in complex porous materials, the mixed-wet state, and its relationship to surface roughness. PNAS, 115(36), 8901 – 8906. DOI: 10.1073/pnas.1803734115.
6. Amott, E. (1959). Observations relating to the wettability of porous rock. Trans. AIME, 216, 156–162.
7. Donaldson, E. C., Thomas, R. D., & Lorenz, P. B. (1969). Wettability determination and its effect on recovery efficiency. Society of Petroleum Engineers Journal, 9(01), 13–20. https://doi.org/10.2118/2338-PA
8. Anderson, W.G. (1986) Wettability literature survey—Part 2: wettability measurement, Soc Petrol Eng JPT 38 (1986) 1246–1262.
9. McPhee, C., Reed, J., and Zubizarreta, I., 2015, Core Analysis: A Best Practice Guide, first edition, Elsevier. ISBN: 9780444635334.
10. Anderson, W. G. (1987)."Wettability Literature Survey Part 5: The Effects of Wettability on Relative Permeability." J Pet Technol 39 (1987): 1453–1468. doi: https://eureka.slb.com:2083/10.2118/16323-PA
11. Masalmeh, S. K. "The Effect of Wettability on Saturation Functions and Impact on Carbonate Reservoirs in the Middle East." Paper presented at the Abu Dhabi International Petroleum Exhibition and Conference, Abu Dhabi, United Arab Emirates, October 2002. doi: https://doi.org/10.2118/78515-MS
12. Virnovsky, G. A., Skjaeveland, S. M., Surdal, J., and P. Ingsøy. "Steady-State Relative Permeability Measurements Corrected for Capillary Effects." Paper presented at the SPE Annual Technical Conference and Exhibition, Dallas, Texas, October 1995. doi: https://eureka.slb.com:2083/10.2118/30541-MS
13. S.K. Masalmeh, and X.D. Jing, Improved Characterisation and Modelling of Carbonate Reservoirs for Predicting Waterflooding Performance", SPE paper 11722_PP, presented at the International Petroleum Technology Conference held in Dubai, U.A.E., December 4–6 (2007).
14. Wilkinson, D., and J. F. Willemsen, Invasion Percolation - a New Form of Percolation Theory, Journal of Physics A: Mathematical and General, 16, 3365-3376, 1983.
15. Masalmeh, S.K., 2001, Experimental Measurements of Capillary Pressure and Relative Permeability Hysteresis, Paper SCA 2001-23 presented at the International Symposium of the Society of Core Analysts, Edinburgh, September.
16. Morrow, N. R. (1975). The effects of surface roughness on contact angle with special reference to petroleum recovery. Journal of Canadian Petroleum Technology, 14(04), 42 – 53. https://doi.org/10.2118/75-04-04
17. Yang, S. Y., Hirasaki, G. J., Basu, S., & Vaidya, R. (1999). Mechanisms for contact angle hysteresis and advancing contact angles. Journal of Petroleum Science and Engineering, 24(2 – 4), 63 – 73. https://doi.org/10.1016/S0920-4105(99)00049-2
18. Melrose, J.C, Wettability as Related to Capillary Action in Porous Media, paper SPE 1085, SPEJ (1965), paper presented at SPE-AlChE Joint Symposium on Wetting and Capillarity in Fluid Displacement Processes, 1959.
19. Toledo, P.G., Scriven, L.E., and Davis, H.T., Pore-Space Statistics and Capillary Pressure Curves From Volume-Controlled Porosimetry, SPEFE (March 1994) 46-54.
20. Longeron, D., Hammervold, W.L., and Skjaeveland, S.M., Water-Oil Capillary Pressure and Wettability Measurements Using Micropore Membrane Technique, SCA 1994-26 presented at the SCA 1994 conference.
21. Anderson, W.G., Wettability Literature Survey – Part 4: Effects of Wettability on Capillary Pressure, JPT (Oct. 1987a) 1283-1300.
22. Anderson, W.G., Wettability Literature Survey – Part 5: The Effects of Wettability on Relative Permeability, JPT (Nov. 1987b) 1453-68.
23. Hirasaki, G.J., Thermodynamics of Thin Films and Three-Phase Contact Regions, Interfacial Phenomena in Oil Recovery, N.R. Morrow (ed.), Marcell Dekker, New York, 23-76, 1991.
24. Kovscek, A.R., Wong, H., and Radke, C.J.: "A pore-level scenario for the development of mixed wettability in oil reservoirs," Am. Inst. Chem. Eng. J. (1993) 39, No. 6, 1072 – 1085.
25. Wardlaw, N.C, The Effects of Geometry, Wettability, Viscosity and Interfacial Tension on Trapping in Single Pore-Throat Pairs, JCPT, May-June 1982, Montreal.
26. Dernaika, Moustafa R., Masalmeh, Shehadeh, Mansour, Bashar, Al Jallad, Osama, and Safouh Koronfol. "Modeling Permeability in Different Carbonate Rock Types." Petrophysics 64 (2023): 18-37. doi: https://doi.org/10.30632/PJV64N1-2023a.
27. Mousavi, M., Prodanovic, M. and Jacobi, D. "New Classification of Carbonate Rocks for Process-Based Pore-Scale Modeling", SPE J. (2013), SPE 163073.
28. Dunham R.J. Classification of Carbonate Rocks According to Depositional Texture. In Classification of Carbonate Rocks: A Symposium. American Association of Petroleum Geologists Memoir 1, ed. W.E. Ham, 108-121. Tulsa, Oklahoma: AAPG (1962)
29. Embry, A.F. and Klovan, J.E. (1971) A Late Devonian Reef Tract on the North Western Banks Island, North West Territories. Bulletin of Canadian Petroleum Geologists, 19, 730-781
30. Leverett, M. C. (1941). Capillary behavior in porous solids. Transactions of the AIME, 142(01), 152 – 169.
31. N.R. Pallas, Y. Harrison, An automated drop shape apparatus and the surface tension of pure water, Colloids and Surfaces, Volume 43, Issue 2, 1990, Pages 169-194, ISSN 0166-6622, https://doi.org/10.1016/0166-6622(90)80287-E.
32. Mirzaei-Paiaman, A. (2022). "Analysis of the bounded and unbounded forms of USBM wettability index". Energy Geoscience. 3 (1): 94–102. doi:10.1016/j.engeos.2021.12.001. S2CID 245108452.
33. Cuiec, L.E., Evaluation of Reservoir Wettability and Its Effects on Oil Recovery, Interfacial Phenomena in Oil Recovery, N.R. Morrow (ed.), Marcell Dekker, New York, 319-75, 1991.

34. Jennings, J.W., and Lucia, F.J., 2003, Predicting Permeability From Well Logs in Carbonates With a Link to Geology for Interwell Permeability Mapping, Paper SPE-84942, SPE Reservoir Evaluation & Engineering, 6(4), 215–225. DOI: 10.2118/84942-PA.

35. Dernaika, M.R., Masalmeh, S.K., Mansour, B., Aljallad, O.A., and Koronfol, S., Geology-Based Modeling of Capillary Pressure in Cretaceous Carbonates Paper presented at the SPE Reservoir Characterisation and Simulation Conference and Exhibition, Abu Dhabi, UAE, January (2023b). doi: https://doi.org/10.2118/212596-MS

36. Dernaika, M. R., AlSumaiti, A. M., and Masalmeh, S. K. "Relative Permeability Trends in Different Dolomite and Limestone Formations." Paper presented at the SPE Advances in Integrated Reservoir Modelling and Field Development Conference and Exhibition, Abu Dhabi, UAE, June 2025. doi: https://doi.org/10.2118/225394-MS

37. Morrow, N. R., "Wettability and Its Effect on Oil Recovery", J. Pet. Tech., 42, 1476 (1990).

38. Al-Khafaji, A., & Buckley, J. S. (2000). "Wettability alteration in dolomite versus limestone: The effect of crude oil composition." SPE Annual Technical Conference and Exhibition. SPE-63171-MS. DOI: 10.2118/63171-MS

39. Standnes, D. C., & Austad, T. (2000). "Wettability alteration in carbonates: Influence of a potential determining cation (Ca^{2+}) and temperature." Colloids and Surfaces A: Physicochemical and Engineering Aspects, 191(1–2), 147–165.

40. Zhang, R., & Austad, T. (2006). "Wettability and oil recovery from carbonates: Effects of temperature and potential determining ions." SPE Journal, 11(3), 280–289. DOI: 10.2118/92999-PA

41. Masalmeh, S.K.: "High Oil Recoveries From Transition Zones", SPE paper 87291 presented at the 2000 SPE Abu Dhabi International Petroleum Exhibition and Conference, Abu Dhabi, 13-15 October.

42. Dernaika, M.R., Basioni, M., Dawoud, A., Kalam, M.Z., and Skjæveland, S.M. "Variations in Bounding and Scanning Relative Permeability Curves with Different Carbonate Rock Types" J. Res. Eval. & Eng. (August 2013).

43. Jerauld, G.R., and Salter, S.J., 1990, Effect of Pore-Structure on Hysteresis in Relative Permeability and Capillary Pressure: Pore-Level Modeling, Transport in Porous Media, 5, 103-151.

44. Honarpour, M., Koederitz, L., and Harvey, A.H., 1987, Relative Permeability of Petroleum Reservoirs, CRC Press Inc, Boca Raton.

45. Jadhunandan, P.P., and Morrow, N.R., 1995, Effect of Wettability on Waterflood Recovery for Crude-Oil/Brine/Rock Systems, Paper SPE-22597, SPE Reservoir Engineering, 10(1), 40-46.

46. Klemin, D., Masalmeh, S., AlSumaiti, A., Bhakta, R., Dernaika, M. (2025). Digital SCAL in Complex Carbonates by the Density Functional Hydrodynamics Method. Proceedings of the 38th International Symposium of the Society of Core Analysts (SCA), Hannover, Germany. DOI: 10.5281/zenodo.16813869

47. Hassler, G.L., Brunner, E., 1945. Measurements of capillary pressures in small core samples. Trans. AIME 192, 10.

48. Forbes, P.L., 1991. Simple and accurate methods for converting centrifuge data into drainage and imbibition capillary pressure curves. In: Society of core analysts annual technical conference August 20-22, San Antonio, paper 9107.

49. El Din, Samy Serag, Dernaika, Moustafa , Hannon, Loay , and Zubair Kalam. "The Effect of Rock Properties on Remaining and Residual Oil Saturation in Heterogeneous Carbonate Rocks." Paper presented at the SPE Middle East Oil and Gas Show and Conference, Manama, Bahrain, March 2013. doi: https://doi.org/10.2118/164141-MS